Scattering of Electromagnetic Waves by Inhomogeneities Excited in a Plasma by a Rapidly Moving Body

Ya. L. Al'pert and L. P. Pitaevskii
Institute of Terrestrial Magnetism, the Ionosphere, and Radio-Wave Propagation; Vavilov Institute of Physical Problems: Academy of Sciences USSR

Results are given of calculations of the scattering function $F_3(\alpha)$ and the effective scattering cross section σ for a body moving rapidly in a plasma in a magnetic field; Strela and BESM-2 computers were used. It is found that σ is represented by a function having many narrow lobes, the main lobe being that corresponding to reflection at a plane having the direction of H_0, the magnetic field. The relation of σ to height and to the wavelength λ is discussed. It is found that the differential cross section can be 1000 m^2 or more for motion at small angles to the direction of the magnetic field.

ONE of the authors[1] has discussed the scattering around (mainly behind) a body moving rapidly in a plasma resulting from perturbations produced in the electron density; estimates[1] show that the effective scattering cross section in the ionosphere can be in excess of 100 m^2, because the magnetic field causes the perturbed region to take a cylindrical form. Later calculations on the perturbations in the electron and ion densities[3] have shown that these can be such as to cause very pronounced scattering of electromagnetic waves. However, a rigorous solution is needed in order to settle the problem. Pitaevskii[2] has used the kinetic equation to derive expressions for the Fourier components of the perturbations, and these give formulas for the effective scattering cross section (allowance is made for the magnetic field, for the collisional frequency, and for the finite size of the body, which is usually much less than the wavelength). Some allowance is also made for the electric potential around the body.

The formulas are very complicated, so a detailed analysis can be performed only on the results of numerical calculations. Here we give such results and analysis for a low density plasma (e.g., the ionosphere), for which the mean free path of the particles is much larger than R_0, the radius of the body, whose speed v_0 is much greater than $(8kT/\pi M)^{1/2}$ (the thermal velocity of the ions) but much less than $(8kT/\pi m)^{1/2}$ (the thermal velocity of the electrons).

Scattering Function

Formulas (69) and (70) of Ref. 2 give the effective differential scattering cross section in a coordinate system coupled to the body as

$$\sigma(\vartheta_1,\vartheta_2,\varphi) = \frac{1}{16}\left(\frac{\omega_0}{c}\right)^4 \frac{R_0{}^4 v_0{}^2}{\Omega_H{}^2} \sin^2\psi_1 F_3(\alpha,\beta,\gamma,\delta) \times |\phi_3(qR_0,\alpha_0)|^2 \quad (1)$$

in which ψ_1 is the angle between the electric field E and the wave vector K' for the scattered wave; ϑ_1, ϑ_2, and φ are angles defining the directions of the incident and scattered waves (Fig. 1). The total effective scattering cross section is

$$\sigma' = \int \sigma(\vartheta_1,\vartheta_2,\varphi)\,do \quad (2)$$

(in which do is an element of solid angle) and is a definite function of these angles.

In formula (1) we have

$$F_3(\alpha,\beta,\gamma,\delta) = \frac{F_1{}^2 + F_2{}^2}{(2 - 2\beta F_1 - \alpha F_2)^2 + (\alpha F_1 - 2\beta F_2)^2} \quad (3)$$

in which

$$F_1 = e^{-\delta}\int_0^\infty \cos\alpha \exp\{-\beta x - \gamma x^2 + \delta\cos x\}dx \quad (4)$$

$$F_2 = e^{-\delta}\int_0^\infty \sin\alpha \exp\{-\beta x - \gamma x^2 + \delta\cos x\}dx$$

$$\alpha = \frac{(qV_0)}{\Omega_H} = b(\cos\vartheta_1\sin\vartheta_2 + \sin\vartheta_1\cos\vartheta_2\cos\varphi) = b\cos\theta \quad (5)$$

and $b = qV_0/\Omega_H$; the vector $\mathbf{q} = (\mathbf{K}' - \mathbf{K})$ is the bisector of the angle between the wave vectors $\mathbf{K}$ and $\mathbf{K}'$ for rays SO and OE from the point of emission S to the object at O and then

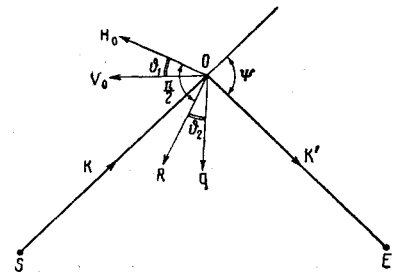

Fig. 1

to the point of observation E. Vector $\mathbf{q}$ lies in the plane of SO and OE, and

$$q^2 = 4\frac{\omega^2}{c^2}\left(1 - \frac{\omega_0{}^2}{\omega^2}\right)\sin^2\frac{\psi}{2} \quad (6)$$

in which ψ is defined as in Fig. 1 (the angle between $\mathbf{K}$ and $\mathbf{K}'$). The scalar products $(\mathbf{v_0H})$ and $(\mathbf{qH})$ define ϑ_1 and ϑ_2:

$$\cos\vartheta_1 = \frac{(\mathbf{V_0H})}{\mathbf{V_0H}} \quad (7)$$

Then ϑ_1 is the angle between the magnetic field $\mathbf{H_0}$ and the velocity $\mathbf{v_0}$, whereas ϑ_2 is the angle between $\mathbf{q}$ and the normal OR to $\mathbf{H_0}$, which lies in the plane of $(\mathbf{qH})$; the latter angle is positive if $\mathbf{q}$ is displaced clockwise with respect to OR. Angle φ is that between the planes of $(\mathbf{v_0H})$ and $(\mathbf{qH})$. In formulas [3 and 4]:

$$\beta = \frac{\nu}{\Omega_H} \qquad \gamma = \frac{a}{2}\sin^2\vartheta_2 \qquad \delta = a\cos^2\vartheta_2 \quad (8)$$

Translated from Geomagnetizm i Aeronomiia (Geomagnetism and Aeronomy) 1, no. 5, 709–724 (1961). Translated by Faraday Translations, New York.

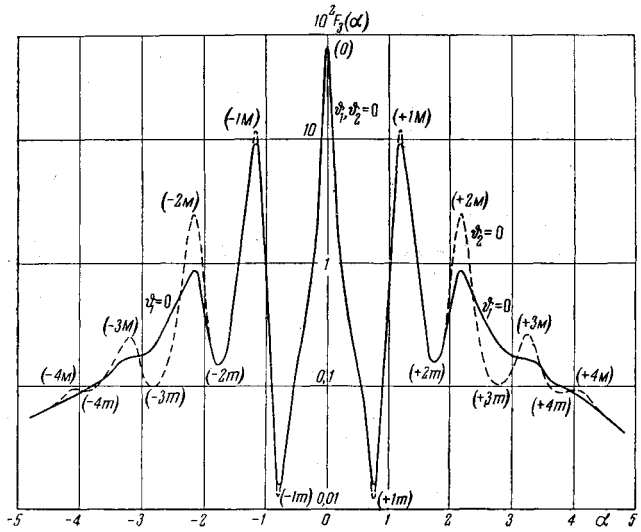

Fig. 2

in which

$$a = \frac{kT}{M\Omega_H^2}\, q^2$$

The parameters α, β, γ, and δ are functions of the six quantities a, b, β, ϑ_1, ϑ_2, and φ, which themselves are dependent on the physical parameters, i.e., on temperature T, magnetic field $\mathbf{H}_0$ (Ω_H), molecular weight of the ions M, collisional frequency ν, wavelength of the radiation $\lambda = 2\pi c/\omega$, angle between $\mathbf{v}_0$ and $\mathbf{H}_0$, and directions of the incident and scattered waves relative to $\mathbf{v}_0$ (or $\mathbf{H}_0$).

This makes the scattering function F_3 very complicated; numerical calculations are essential. Function ϕ_3 takes account of the finite size of the body.

It has been shown[2] that

$$\phi_3 = \phi_1^2 + \phi_2^2 \tag{9}$$

in which

$$\phi_1 = 2\int_0^{\pi/2} \sin\vartheta \cos\vartheta \cos\{qR_0 \cos\vartheta \cos\theta\} \times J_0(qR_0 \sin\vartheta \sin\theta)\, d\vartheta \tag{10}$$

$$\phi_2 = 2\int_0^{\pi/2} \sin\vartheta \cos\vartheta \sin\{qR_0 \cos\vartheta \cos\theta\} \times J_0(qR_0 \sin\vartheta \sin\theta)\, d\vartheta$$

Here J_0 is the Bessel function of zero order and

$$\mathbf{qV}_0/qV_0 = \cos\theta \tag{11}$$

We have tabulated the function of (3) for values of α, β, γ, and δ, and this has enabled us to examine the effects of height, wavelength, temperature, and direction of motion. These

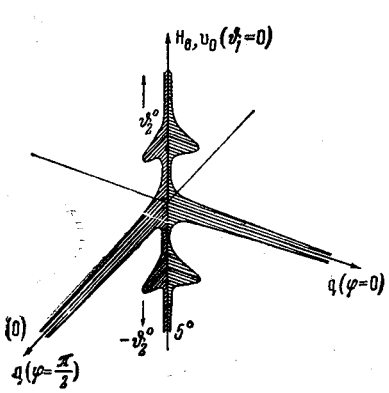

Fig. 3

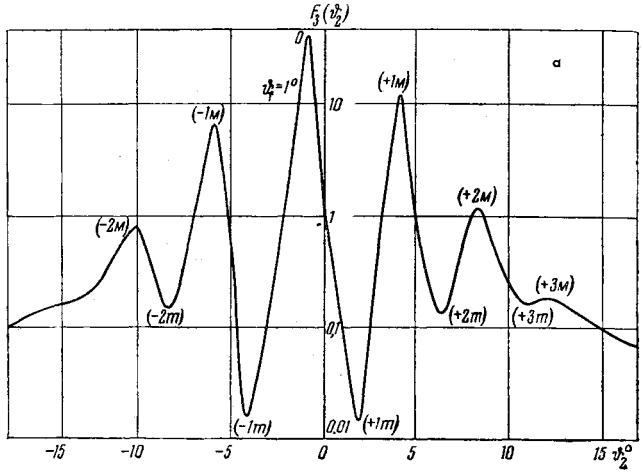

Fig. 4a

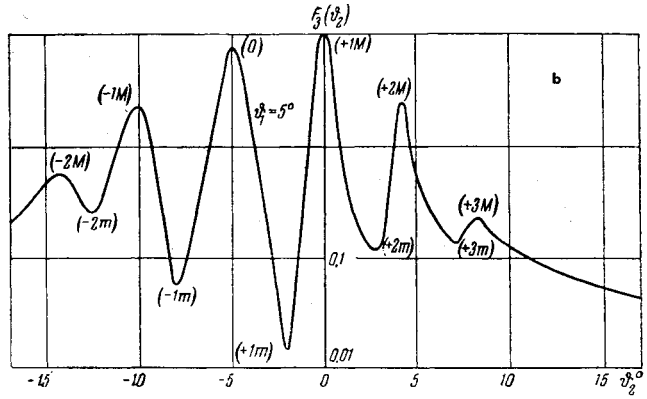

Fig. 4b

are dealt with in the following sections; first we consider some general features of F_3.

The main feature is that F_3 is oscillatory, with maxima and minima at certain values of α. The values of a, b, β, and γ we used give six to eight maxima and the same number of minima, which are symmetrically disposed with respect to the main peak if $\vartheta_1 = 0$. The main peak, which we call the peak of order (0), corresponds to

$$\alpha = 0 \tag{12}$$

The secondary peaks and the minima are denoted respectively by $(\pm 1M)$, $(\pm 2M)$, $(\pm 3M)$, . . . and $(\pm 1m)$, $(\pm 2m)$, $(\pm 3m)$, and so on; if $\vartheta_1 = 0$, they lie at

$$\alpha_{\max} \simeq \pm 1.22,\ \pm 2.18\ \pm 3.15,\ \pm 4.23$$

$$\alpha_{\min} \simeq \pm\ 0.73,\ \pm 1.70,\ \pm 2.91,\ \pm 3.86 \tag{13}$$

The main peak in F_3 for $\alpha_0 = 0$ is largest when $\vartheta_1 = 0$ or $\vartheta_2 = 0$; this peak may be smaller than the first-order peaks ($\alpha_{\max} = +1.22$) for other ϑ_1 and ϑ_2, but it is always larger

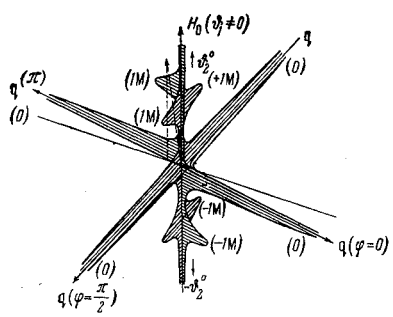

Fig. 5

Table 1 $\left\{\frac{1}{16}\left(\frac{\omega_0}{c}\right)^4 \frac{R_0^4 v_0^2}{\Omega H^2} \sin^2\psi_1\right\}$

	Day			Night		
	z, km			z, km		
R_0, m	300	400	700	300	400	700
0.5	$1.8\cdot10^{-2}$	$1.2\cdot10^{-2}$	$1.2\cdot10^{-3}$	$6\cdot10^{-5}$	$1.2\cdot10^{-3}$	$1.8\cdot10^{-4}$
1	0.3	0.2	$2\cdot10^{-2}$	10^{-3}	$2\cdot10^{-2}$	$3\cdot10^{-3}$
2	4.8	3.2	0.32	$1.6\cdot10^{-2}$	0.32	$4.8\cdot10^{-2}$
3	24	16	1.6	$8\cdot10^{-2}$	1.6	0.24

Fig. 6

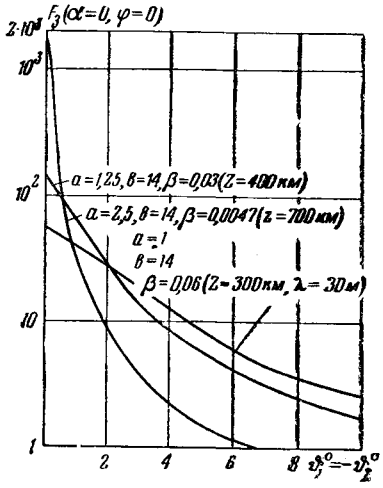

Fig. 7

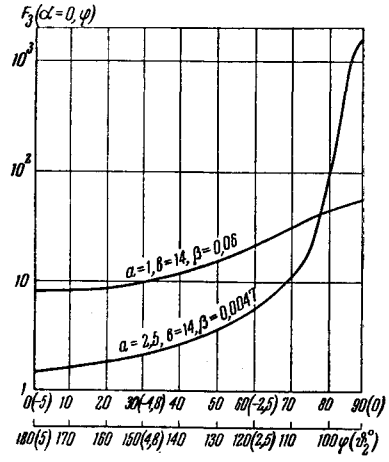

than the others if $\vartheta_1 = 0$ (i.e., if $\mathbf{v}_0$ and $\mathbf{H}_0$ are collinear). The number of secondary peaks is very much dependent on β and γ, which govern the convergence of the integrals in (4); the most important term here is the quadratic term containing γ in (4). For example, $a = 1$ ($z = 300$ km, $\lambda = 30$ m) corresponds to loss of the third-order peak ($\alpha \approx 4.24$, $\vartheta_2 \approx 17.5$) for $\vartheta_1 = 0$, but the third- and fourth-order peaks remain appreciable in this case if $\vartheta_2 = 0$. Figure 2 shows two curves for $F_3(\alpha)$ for $a = 1$, $\beta = 0.06$, and $b = 14$; the results may be examined in more detail by reference to the tables in the next section.

$F_3(\alpha)$ is independent of φ [see (5)] if $\vartheta_1 = 0$ ($\mathbf{v}_0 \| \mathbf{H}_0$), and the surface for $F_3(\alpha, \varphi)$ is formed by rotating the curve of Fig. 2 about the axis of ϑ_0 (or $\mathbf{H}_0$). Figure 3 shows the three-dimensional representation of $F_3(\vartheta_2, \varphi)$ for $\vartheta_1 = 0$ (here $\mathbf{H}_0 \| \mathbf{v}_0$, $a = 1$, $b = 14$, and $\beta = 0.06$) as sections in the planes $\varphi = 0$ and $\varphi = \pi/2$. Here the axis of φ_2 is vertical, because the rapid variation in $F_3(\varphi_2)$ makes it difficult to represent the surface in polar coordinates, so details of the structure are not revealed.

Figures 2 and 3 make it clear that F_3 varies rapidly with ϑ_2 (or with ϑ_1 if ϑ_2 is fixed); the main and secondary peaks have widths of 1–2°. The width of the main peak becomes less as the height of the peak increases (this corresponds to increase in a and decrease in β, i.e., to increase in the height; see Tables 1–7); the ratios to the other peaks also increase.

Figure 2 shows $F_3(\alpha)$ on a logarithmic scale, which tends to minimize the rapid variations; $F_3(\alpha)$ ceases to be symmetrical with respect to ϑ_2 if $\vartheta_1 \neq 0$, for then α is dependent on φ. Here $\alpha = 0$ corresponds for a given $\varphi \neq \pi/2$ to a negative ϑ_2 [see (5)], so the main peak falls below the plane $\vartheta_2 = 0$; the lines circumscribing the surface of the main peak in $F_3(\vartheta_2, \varphi)$ are then no longer circles in the plane $\vartheta_2 = 0$ (as for the case $\vartheta_1 = 0$) but are spatial curves of elliptic type that meet the plane $\vartheta_2 = 0$ when ϑ is $\pi/2$ or $3\pi/2$. At these two points the main peak has the height for $\vartheta_1 = 0$.

Figure 4 shows $F_3(\vartheta_2)$ for $\varphi = 0$ and $\vartheta_1 \pm 0$; here $a = 1$, $b = 14$, and $\beta = 0.06$ ($z = 300$ km, $\lambda = 30$ m), with $\vartheta_1 = 1.5°$. The orders of the peaks and troughs are shown.

Figure 5 shows $F_3(\vartheta_2, \varphi)$ in the mutually perpendicular planes $\varphi = 0$ and $\varphi = \pi/2$ for $a = 1$, $b = 14$, $\beta = 0.06$, and $\vartheta_1 \neq 0$.

Figures 6 and 7 show the behavior of the main peak for $\alpha = 0$ as a function of $\vartheta_1 = -\vartheta_2$ in the plane $\varphi = 0$ and also as a function of φ for $\vartheta_1 = 5°$. The peak height clearly increases as φ goes from 0 to $\pi/2$ and corresponds to ϑ_2 negative; it is maximal and equals that for $\vartheta_1 = 0$, the maximum lying in the plane $\vartheta_2 = 0$, when $\varphi = \pi/2$. The fall in the peak height for φ between $\pi/2$ and π is symmetrical; the peak corresponds to ϑ_2 positive, and identical values of F_3 for $\alpha = 0$ correspond in pairs to $\varphi = \pi/2 + \varphi_M$, $\vartheta_2 = \vartheta_{2m}$ and $\varphi = \pi/2 - \varphi_M$, $\vartheta_2 = -\vartheta_{2M}$.

The value for ϑ_{2M} is governed by the condition $\alpha = 0$ for a given φ_M [see (5)]. The higher-order peaks are similarly affected for $\vartheta_1 = 0$; (5) gives their ϑ_2 and φ for given ϑ_1.

These general features of F_3 enable us to consider the behavior of σ as the body passes over the point of observation.

Table 2 $\phi_3\left(\frac{4\pi R_0}{\lambda}, 0, 0, 0\right)$

$4\pi R_0/\lambda$	0	0.05	0.1	0.2	0.3	0.4	0.5	0.6
ϕ_3	1.00	0.999	0.995	0.99	0.97	0.96	0.94	0.91
$4\pi R_0/\lambda$	0.7	0.8	0.9	1.0	1.5	2.0	2.5	3
ϕ_3	0.88	0.84	0.81	0.77	0.55	0.33	0.16	0.05
$4\pi R_0/\lambda$	3.5	3.83	4	4.5	5	5.5	5.54	6
ϕ_3	$6\cdot10^{-3}$	...	$1.2\cdot10^{-3}$	$1.1\cdot10^{-2}$	$1.7\cdot10^{-2}$	$1.6\cdot10^{-2}$	$1.6\cdot10^{-2}$	$8\cdot10^{-3}$
$4\pi R_0/\lambda$	6.5	7.01	7.5	8	8.5	8.64	9	9.5
ϕ_3	$2.2\cdot10^{-3}$	...	$1.3\cdot10^{-3}$	$3.4\cdot10^{-3}$	$4.1\cdot10^{-3}$	$4\cdot10^{-3}$	$3\cdot10^{-3}$	$1.2\cdot10^{-3}$

Table 3 $F_3(\vartheta_2, \vartheta_1)$ **for** $\lambda = 30$ m, $\varphi = 0$

	$\vartheta_1 = 0$			$\vartheta_2 = 0$			$\vartheta_1 = -\vartheta_2$		
	z, km			z, km			z, km		
ϑ_1, ϑ_2	300	400	700	300	400	700	300	400	700
0	53.46	134.4	1535	53.46	134.4	1535	53.46	134.4	1535
0.02	...	...	613.9	...	...	...	...	...	...
0.03	...	...	355.1	...	...	...	...	...	...
0.05	49.20	103.2	150.7	...	...	...	...	...	...
0.1	39.72	60.86	40.8	...	...	...	...	...	...
0.2	22.44	23.10	10.31	...	23.07	10.0	...	...	...
0.3	12.98	11.30	4.56	...	...	4.42	...	...	...
0.5	5.44	4.20	1.58	5.39	4.14	1.53	49.62	101.1	109.6
1.0	1.32	0.94	0.32	1.30	0.92	0.31	41.25	61.65	32.14
1.5	0.47	0.31	...	...	...	...	...	...	...
2.0	0.17	0.10	0.019	0.17	0.099	0.018	...	...	9.30
3.0	0.015	0.011	0.037	0.013	$7.8\cdot10^{-3}$	0.023	...	14.01	3.99
3.5	0.15	0.18	...	...	...	...	...	...	...
4.0	0.85	0.67	0.56	0.98	0.69	0.68	...	...	...
4.5	2.48	2.22	1.30	...	...	...	...	...	...
5.0	9.39	13.18	3.18	10.26	12.61	3.41	7.95	5.85	1.48
5.5	2.58	2.71	1.29	...	...	...	...	...	...
6.0	0.88	1.44	0.28	0.77	0.61	0.19	5.96	4.23	...
7.0	0.18	0.10	0.025	0.18	0.11	0.010	4.63	3.20	...
8	0.22	0.18	0.14	0.26	0.053	0.10	3.71	2.52	...
9	0.89	0.98	0.45	2.48	5.31	28.9	3.04	2.03	...
9.5	0.83	1.15	0.62	0.78	1.05	1.57	...	...	...
10	0.53	0.70	0.53	0.45	0.52	0.47	2.54	1.68	0.39
11	0.25	0.25	0.21	0.23	0.22	...	...	...	...
12	0.19	0.19	0.18	0.10	0.046	...	...	...	...
12.5	0.187	0.20	...	0.32	0.89	...	...	...	...
13	0.18	0.21	0.24	0.28	0.47	...	...	...	...
13.5	0.17	0.21	0.25	0.19	0.25	...	...	...	...
14	0.16	0.19	0.25	0.16	0.19	...	...	...	...
15	0.12	0.14	0.20	0.12	0.13	...	...	...	...
16	0.10	0.11	...	0.088	0.086	...	...	...	...
16.5	...	...	...	...	0.058	...	...	...	...
17	...	0.091	...	0.091	0.16	...	...	...	...
17.5	0.077	...	...	0.080	0.020	...	...	...	...
18	0.071	0.078	...	0.072	0.16	...	...	...	...
18.5	0.067	...	...	0.067	...	...	...	...	...
19	0.062	0.067	...	0.062	0.070	...	...	...	...
20	0.054	0.058	...	0.054	0.057	...	...	...	...
21	...	...	...	0.048	...	...	...	...	...
22	...	...	...	0.044	...	...	...	...	...
23	...	...	...	0.039	...	...	...	...	...
24	...	...	...	0.036	...	...	...	...	...

Table 4 $F_3(\vartheta_2)$ **for** $\vartheta_1 = 0$ **near the main peak for** $\varphi = 0$ **as a function of** λ **and** z

	$z = 300$ km				$z = 400$ km				$z = 700$ km		
	λ, m				λ, m				λ, m		
$\vartheta_2{}^0$	30	20	15	10	30	20	15	10	30	20	15
0	53.46	11.07	4.82	1.72	134.4	31.05	14.10	5.20	1535	479.3	241.3
0.02	...	...	...	...	...	...	...	...	613.9	...	...
0.03	...	...	...	0.080	...	...	...	0.063	355.1	...	...
0.05	49.20	9.75	3.96	...	103.2	20.54	7.71	...	150.7	25.3	8.67
0.1	39.72	7.16	2.58	...	60.86	10.2	8.27	...	40.8	6.58	2.20
0.2	22.44	3.46	...	...	23.10	3.36	...	...	10.3	1.63	...
0.3	12.98	1.83	0.51	...	11.30	1.55	0.42	...	4.56	0.70	...
0.5	5.44	0.68	0.16	0.016	4.20	0.52	0.12	0.011	1.58	0.22	0.056
1.0	1.32	0.11	0.01	0.020	0.94	0.074	0.005	0.017	0.32	0.027	0.001
1.5	0.47	...	0.03	...	0.31	...	0.027	...	...	$8\cdot10^{-5}$	0.023
2	0.17	0.031	0.48	0.016	0.10	$3.6\cdot10^{-3}$	...	0.010	0.019	0.026	...

Table 5 Height of the main peak in F_3 **for** $\alpha = 0$ **as a function of** φ **for** $\vartheta_1 = 5°$

φ,^{0}	0	15	30	60	75	90	105	150	180
$\vartheta_2{}^0$	−5	−4.8	−4.3	−2.5	−1.3	0	1.3	4.3	5
				$z = 300$ km					
F_3	7.95	8.38	9.88	20.38	35.98	53.46	35.98	9.88	7.95
				$z = 700$ km					
F_3	1.48	...	...	5.67	19.74	1535	19.74	...	1.48

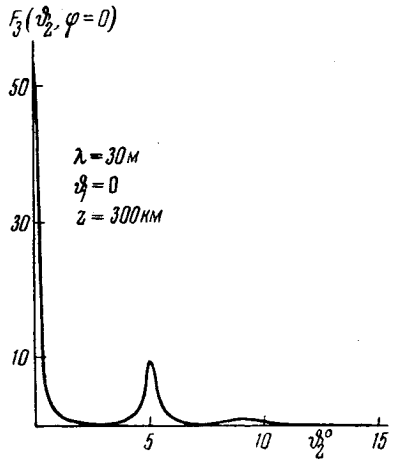

Fig. 8

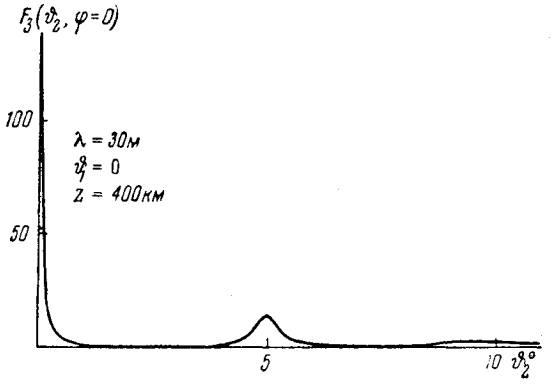

Fig. 9

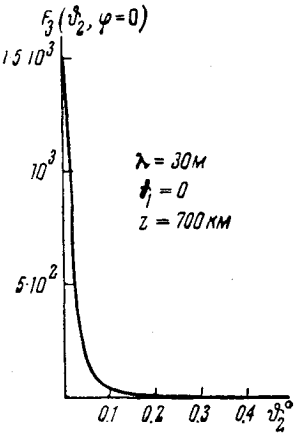

Fig. 10

Effective Scattering Cross Section as a Function of Height and Wavelength

The effective cross section is determined by **K′** (Fig. 1) as the body passes over the point of observation and by the incident field direction **K**; it is the product of three factors:

$$\sigma = \left\{\frac{1}{16}\left(\frac{\omega_0}{c}\right)^4 \frac{R_0^4 V_0^2}{\Omega_H^2} \sin^2\psi_1\right\} F_3(a, b, \beta, \vartheta_1, \vartheta_2, \varphi)\phi \times \left(\frac{4\pi R_0}{\lambda}, \vartheta_1, \vartheta_2, \varphi\right) \quad (14)$$

We have tabulated F_3 and ϕ_3 for various values of the parameters in order to examine the behavior of σ; the heights z used were 300, 400, and 700 km. In conjunction with the known properties of the ionosphere[4] and $v_0 = 8$ km/sec, we have derived values for the first factor in (14) (Table 1).

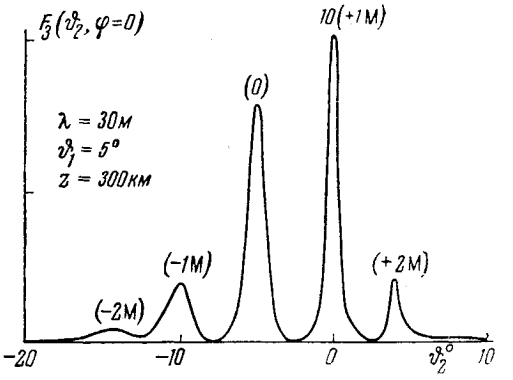

Fig. 11

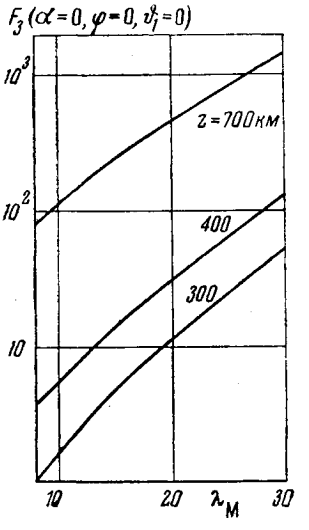

Fig. 12

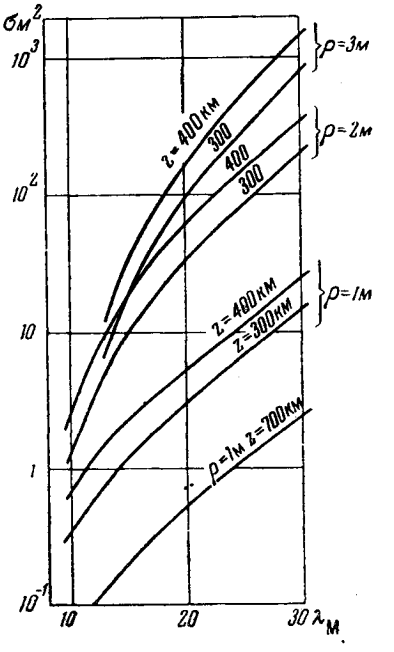

Fig. 13

The third factor in (9) is principally a function of R_0/λ. We have computed it only for $\vartheta_1 = \vartheta_2 = \varphi = 0$ (i.e., for the main peak in F_3; see Table 2). Here

$$\phi_3 = \left[\frac{J_1(4\pi R_0/\lambda)}{4\pi R_0/\lambda}\right]^2$$

Formula (10) shows that the behavior of $\phi_3(4\pi R_0/\lambda)$ for other values is much the same. Fairly detailed values have

Table 6 Heights of peaks (0) and (+1M) in F_3 as functions of T and z for $\lambda = 30$ m

	z = 300 km				z = 400 km			
	T^0	800	1660	2000	T^0	1000	2000	
ϑ_1^0	= {0	{53.46	14.04	9.67	ϑ_1^0	= {0	{134.4	{38.14
	{5	{10.26	4.12	...		{5	{ 12.61	{ 3.16
ϑ_2^0	= 0	...	...	...	ϑ_2^0	= 0	...	...
ϑ_1^0	= 0	9.39	2.57	...	ϑ_1^0	= 0	13.18	2.2
ϑ_2^0	= 5	...	...	...	ϑ_1^0	= 5	...	...

Table 7 Effective cross sections σm² for inhomogeneities in the direction of the main peak and σ_0m² for a metallic sphere in the reverse direction

	z = 300 km				z = 400 km				z = 700 km			
	λ, m				λ, m				λ, m			
R_0, m	30	20	15	10	30	20	15	10	30	20	15	10
						Day						
0.5 σ	0.97	0.19	0.08	0.03	1.60	0.36	0.16	0.06	0.16	0.04	0.02	$6\cdot10^{-3}$
σ/σ_0	1380	47.5	7.3	0.5	2290	90	14.4	1	229	9	1.4	0.1
1 σ	15.4	3.01	1.18	0.34	25.9	5.64	2.31	0.68	2.6	0.56	0.2	0.07
σ/σ_0	350	13.7	1.6	0.1	587	25.4	3.2	0.22	59	2.5	0.32	0.02
2 σ	210	35.0	10.2	1.32	352	65.5	19.8	2.66	35.2	6.5	2.0	0.27
σ/σ_0	72	2.8	0.32	0.04	121	5.2	0.63	0.08	12	0.5	0.06	$8\cdot10^{-3}$
3 σ	810	98.0	18.5	0.04	1420	184	35	0.08	142	18.4	3.5	$8\cdot10^{-3}$
σ/σ_0	28.5	1.1	0.26	$6\cdot10^{-3}$	50	2.1	0.5	$3\cdot10^{-4}$	5	0.2	0.05	$3\cdot10^{-5}$
						Night						
0.5 σ	$3\cdot10^{-3}$	$7\cdot10^{-4}$	$2\cdot10^{-4}$	10^{-4}	0.16	0.04	0.02	$6\cdot10^{-3}$	10^{-2}	$2\cdot10^{-3}$	$8\cdot10^{-4}$	$3\cdot10^{-4}$
σ/σ_0	4.3	0.17	0.02	$1.6\cdot10^{-3}$	229	9	1.4	0.1	14	0.5	0.07	$5\cdot10^{-3}$
1 σ	0.05	10^{-2}	$3\cdot10^{-3}$	10^{-3}	2.6	0.56	0.2	0.07	0.15	$3\cdot10^{-2}$	10^{-2}	$3\cdot10^{-3}$
σ/σ_0	1.1	0.05	0.014	$3\cdot10^{-4}$	59	2.5	0.32	0.02	3.4	0.14	0.013	10^{-3}
2 σ	0.7	0.1	0.03	$3\cdot10^{-3}$	35.2	6.5	2.0	0.27	2.1	0.35	0.10	0.01
σ/σ_0	0.24	$3\cdot10^{-3}$	$2.4\cdot10^{-3}$	$9.6\cdot10^{-5}$	12	0.5	0.06	$8\cdot10^{-3}$	0.72	0.03	$3\cdot10^{-3}$	$3\cdot10^{-4}$
3 σ	2.7	0.33	0.66	10^{-4}	142	18.4	3.5	$8\cdot10^{-3}$	8.1	0.98	0.18	$4\cdot10^{-4}$
σ/σ_0	0.1	$3.6\cdot10^{-3}$	$6.6\cdot10^{-4}$	$1.4\cdot10^{-5}$	5	0.2	0.05	3.10^{-5}	0.35	$1.1\cdot10^{-3}$	$2.5\cdot10^{-3}$	$1.5\cdot10^{-6}$

been derived for the factor F_3 in (14) as a function of ϑ_1, φ_2, and φ, for this is the main factor. This knowledge of F_3 enables us to examine the behavior of σ under various conditions.

The foregoing section shows that the main peak in σ lies in the direction corresponding to mirror-image reflection from the direction of the earth's magnetic field for $\vartheta_1 = 0$ ($\mathbf{v}_0 \| \mathbf{H}_0$). Here the vector $\mathbf{q}$ coincides with the normal to $\mathbf{H}_0$, but it is turned relative to that normal if $\vartheta_1 \pm 0$ through an angle $\pm\vartheta_2$, which is found from (5) for $\alpha = 0$ for given ϑ_1 and ϑ. That is, $\mathbf{q}$ lies at an angle $\pi/2 \pm \vartheta_2$ to $\mathbf{H}_0$. For example, the main peak lies along $\mathbf{K}'$ if $\vartheta_1 = 5°$ and $\varphi = 0$, this $\mathbf{K}'$ being chosen to set $\mathbf{q}$ at $\pi/2$–5° to $\mathbf{H}_0$. The ϑ_2 for the higher-order peaks are given by the $\alpha_{\max}$ [see (10)] in conjunction with (5); for example, the values for peaks of order up to the third for $\varphi = 0$, $\vartheta_1 = 0$, and $b = 14$ are

$$\vartheta_{2\,\max} \approx 0°, \pm5°, \pm9°, \pm13° \qquad (15)$$

whereas for $\vartheta_1 = 1°$, $\varphi = 0$, and $b = 14$ we have

$$\vartheta_{2\,\max} \approx -1°, (+4°, -6°), (+8°, -10°), (+12°, -14°) \qquad (16)$$

Tables 3–5 and Figs. 8–13 show the behavior of F_3 as a function of λ, ϑ_1, ϑ_2, φ, and z; some $F_3(\vartheta_2)$ curves for $\varphi = 0$ are for $\lambda = 30$ m, $\vartheta_1 = 0$, and z of 300, 400, and 700 km (Figs. 8–10) and for $z = 300$ km and $\vartheta_1 = 5°$ (Fig. 11). These $F_3(\vartheta_2)$ curves for $\varphi = 0$ differ from those of Figs. 2 and 4 in being on a linear scale; they show clearly the widths of the various peaks. Figure 12 shows the height of the main peak as a function of λ; Table 4 enables one to evaluate the width for various λ.

Any change in T (and hence in ν) naturally affects α and β [see (7) and (8)]; Table 6 gives an indication of the effects of T on F_3.

Table 7 and Fig. 13 (part) give the height of the main peak in σ for various z and λ for R_0 of 0.5, 1, 2, and 3 m (spherical bodies); Table 7 also gives the ratio of σ to the effective cross section of a sphere of the corresponding size in the reverse direction. This σ/σ_0 indicates the relative magnitude of the scattering caused by the inhomogeneities around the body. The differential effective cross section for the main peak $\sigma(0,0)$ is sometimes much greater than σ_0 during daylight hours; it may be hundreds of square meters. The values in Table 7 relate only to one direction, however, so that we must consider also the effects of the width of the lobe. This is done in the next section, where it is shown that the scattering can be high for short intervals as the object passes over the point of observation. A metal sphere scatters more nearly isotropically; therefore the time for which it produces a signal is more or less the time it takes to pass through the directional pattern of the antenna.

Table 7 also shows that the strongest scattering occurs at around 400 km in the region between 300 and 700 km; it varies roughly as $\exp(-1/\lambda)$ and is virtually negligible for $\lambda < 15$ m. The effective cross section at night is much smaller, being appreciable only for λ of 20–30 m at the optimal height.

The effect is almost independent of the properties and shape of the body; $\mathbf{v}_0$ and R_0 are the only important parameters. On the other hand, the scattering by the body itself is dependent on the properties; in this respect a smooth metal sphere is the best at these wavelengths, and bodies of the same size but with other surfaces have much lower σ_0. Further, σ/σ_0 increases rapidly as R_0 decreases; for $2\pi R_0/\lambda \ll 1$, we have

$$\sigma_0 \rightrightarrows \frac{16\pi^4 R_0^6}{\nu^4} \qquad \sigma \approx R_0^4 \qquad \frac{\sigma}{\sigma_0} \approx \frac{1}{R_0^2} \to \infty$$

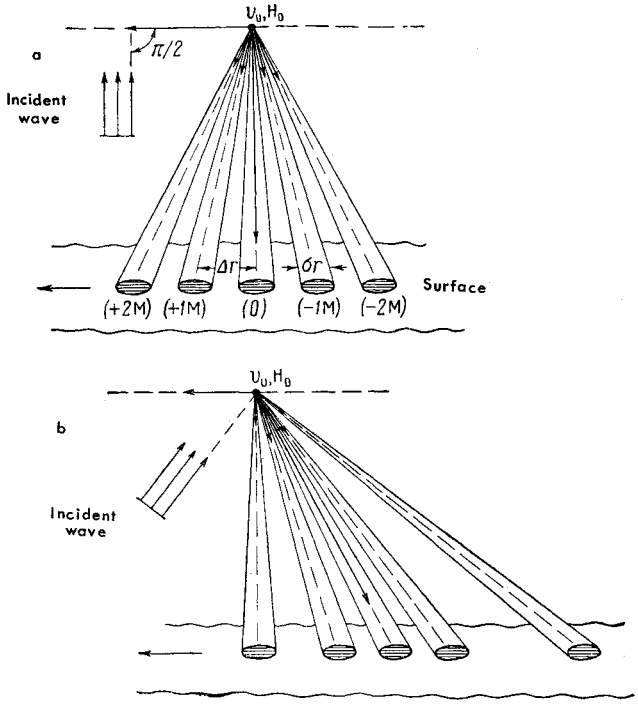

Figs. 14 a and b

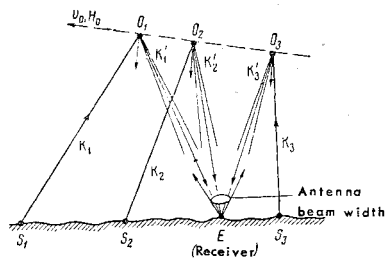

Fig. 15

Scattered-Wave Field at the Point of Observation

Here we give the general picture and survey the results. We assume that v_0 lies along $\mathbf{H}_0$ and that $\mathbf{K}$ is normal to $\mathbf{H}_0$ (or v_0); the surface of rotation formed by the scattered field around v_0 or $\mathbf{H}_0$ has several lobes, and here the main lobe lies along the normal to v_0, the other lobes being symmetrically placed. The total angle covered by the several lobes is only 15–20° (relative to the normal to $\mathbf{H}_0$), after which the intensity falls off monotonically with ϑ_2. Thus the effect seen at a point on the ground as the body approaches is as follows. The scattered field at first increases monotonically; then follow peaks associated with the positive lobes (. . . , $+2M$, $+1M$), the main peak (0), the peaks for the negative lobes ($-1M$, $-2M$, . . .), and finally a monotonic decrease. Now σ is large only within the main lobe and one or two side lobes, so the scattered field is reasonably strong only for a few short intervals. Consider, for example, the case z = 400 km; here $\sigma \approx 350$ m² for the main lobe for $\lambda = 30$ m and $R_0 = 2$ m, if the width of the main lobe is defined as that corresponding to $\sigma = \sigma_0$, in which case $\delta\vartheta_2 \approx 1°$ (Fig. 9). The distance corresponding to this at the given height is $\delta r \approx z\delta\vartheta_2 \approx 4$ km, so the transit time is $\delta t \approx v_0/\delta r \approx 0.5$ sec, during which time the mean intensity corresponds to $\sigma \approx$ 170 m², because $\sigma(\vartheta_2)$ varies nearly linearly within this range in ϑ_2. The ($\pm 1M$) peaks are reasonably strong, because σ is comparable with σ_0 for these, but the higher-order lobes are difficult to detect against the background of scattering from the body itself. That is, the scattering effect is seen as three peaks in the intensity in this case. Of course, changes in the size, nature, and shape of the body can alter this picture substantially, as can change in the sensitivity of the detector.

Figure 14a shows how the various scattering lobes appear at the ground when $v_0 \| \mathbf{H}_0$ and the incident wave is normal to v_0; Fig. 14b does the same for a wave inclined to v_0. In the latter case all lobes are turned relative to the normal to the magnetic field, the main lobe taking the direction of the mirror-image reflection from $\mathbf{H}_0$.

Now we consider a body moving at a certain (fairly small) angle to the magnetic field. The surface representing the scattered wave is here more complicated, and the elements of the surfaces of the lobes are curved, although the general character of the wave as seen at the ground is much the same. The detailed changes may be very substantial. For example, if rays OS and OE of Fig. 1 lie in the plane of v_0 and $\mathbf{H}_0$ ($\varphi = 0$ or π), there are more low intensity lobes (Fig. 11). Again, if OS and OE lie in a plane normal to the other plane ($\varphi = \pi/2$ or $3\pi/2$), the field at the main peak is as for $v_0 \| \mathbf{H}_0$. That is, if emission and reception are performed in a plane normal to the plane of ($v_0\mathbf{H}_0$), the scattered intensity is the same as if the two planes are the same.

Table 8 gives results for the intensity peaks as seen at the ground for various λ and z for fields greater than or comparable with those produced by a metal sphere of the corresponding size. The δr and $\delta t = v_0/\delta r$ the width of the illumi-

Table 8 Characteristics of signal peaks as received by scattering from the track during the day for $\vartheta_1 = 0$

	Parameters						Parameters				
λ, m	R_0, m	Peak no.	σ/σ_0	δt, sec	δr, km	Δt, sec	λ, m	R_0, m	Peak no.	σ/σ_0	δt, sec	δr, km
		z = 300 km							z = 700 km			
30	1	(0)	175	0.6	5	. . .	30	1	(0)	29	. . .	. . .
		($\pm 1M$)	35	. . .	. . .	3.4		2	(0)	6	0.15	1.2
	2	(0)	36	1	8	. . .		3	(0)	2.5	0.2	1.8
		($\pm 1M$)	7.5	0.8	. . .	3.4			z = 300 km			
	3	(0)	14	1.2	9	. . .		1	(0)	6.8	. . .	. . .
		($\pm 1M$)	2.8	1.0	. . .	3.4	20	2	(0)	1.4	0.25	2
		z = 400 km						3	(0)	0.6	0.3	2
30	1	(0)	293	0.4	3.5	. . .			z = 400 km			
		($\pm 1M$)	29	. . .	. . .	4.5	20	1	(0)	12.7	. . .	. . .
						. . .		2	(0)	2.6	0.25	2
	2	(0)	60	0.8	6.5	. . .		3	(0)	1.0	0.25	2
		($\pm 1M$)	6	0.4	3.5	4.5						
	3	(0)	25	1.3	11	. . .						
		($\pm 1M$)	2.5	1.3	. . .	4.5						

nated area and the duration of the effect at the receiving point and Δt is the interval between successive peaks at that point.

Table 8 shows that Δt is several seconds, whereas δt is less than 1 sec. This is strictly true, of course, only if the body is exposed to plane waves from one direction only; transmitters at several points S_1, S_2, S_3 (Fig. 15) give rise to several scattered waves at point E, so that the effect lasts for a substantially longer time.

Finally, σ exceeds σ_0 only for bodies of small size if there is no magnetic field; for example, $\sigma_{max} \approx 0.005$ m^2 for $\lambda = 30$ m, $z = 300$ km, and $R_0 = 0.5$ m, so that $\sigma_{max}/\sigma_0 \approx 7$ (ionization produces much the greater scattering), whereas $\sigma_{max} \approx 0.02$ m^2 and $\sigma_{max}/\sigma_0 \approx 0.5$ for $R_0 = 1$ m, so that the sphere scatters more than the track. Further, σ varies as $1/\epsilon$ if the dielectric constant of the plasma ϵ alters; therefore, the effect should be substantially greater if the body lies in a region in which ϵ approaches zero. However, this last case demands special examination; no precise deductions of the behavior of σ as $\epsilon \rightarrow 0$ are possible without a detailed analysis.

—*Received August 4, 1961*

References

[1] Al'pert, Ya. L., Usp. Fiz. Nauk (Soviet Phys.-Usp.) **71**, 369 (1960).

[2] Pitaevskii, L. P., Geomagnetizm i Aeronomiia (Geomagnetism and Aeronomy) **1**, no. 2, 194–208 (1961).

[3] Gurevich, A. V., Trudy IZMIRAN (Trans. Inst. of Terrestrial Magnetism, the Ionosphere, and Radio-Wave Propagation) **17** (23), 173; *Iskusstvennye Sputniki Zemli* (*Artificial Earth Satellites* 1961), no. 7, p. 101.

[4] Al'pert, Ya. L., *Rasprostranenie Radiovoln i Ionosfera* (*Propagation of Radio Waves and the Ionosphere*) (Academy of Sciences Press, USSR, 1960).

Reviewer's Comment

The results of a previous contribution* are used to present numerical results (based on computer calculations) on the scattering cross section of a wake induced by a spherical satellite vehicle traversing typical regions of the ionosphere. The influence of a magnetic field is specifically included. Effects of height, frequency, ion temperature, vehicle velocity, and geometry (direction of magnetic field, vehicle velocity, and earth stations) are illustrated by the calculations.

The contribution is noteworthy in that at least three significant conclusions can be drawn from the numerical results. These are:

1) The scattering cross section is a maximum at the mirror image reflecting points only when the vehicle velocity is parallel to the magnetic field.

2) When the vehicle velocity is not parallel to the magnetic field, major maxima occur at angles off the specular direction, the deviation depending upon vehicle velocity and scattering angle of the wave.

3) A series of maxima and minima in the scattering cross section occurs. These form a symmetrical sequence if the vehicle moves parallel to the magnetic field, but are notably unsymmetrical (in magnitude) at other directions of the vehicle motion relative to the magnetic field.

An attempt to interpret high frequency radio reflections observed from orbiting satellites† in terms of this theory and radio observations designed to verify these predictions would form a worthy contribution in the future.

—M. P. Bachynski
Director, Microwave Research Laboratory
RCA Victor Company Ltd.
Montreal, Canada

* Pitaevskii, L. P., Geomagnetizm i Aeronomiia (Geomagnetism and Aeronomy) **1**, no. 2, 194–208 (translated on pp. 994–1000 of this issue). Unfortunately the notation used in the foregoing review and the present article are somewhat different.

† For instance: Krauss, J. D., et al., Proc. Inst. Radio Engrs. **48**, 672–678, 1913–1914 (1960).

APRIL 1963 AIAA JOURNAL VOL. 1, NO. 4

Analog Computer Solution of the Problem of Accumulation of Perturbations

G. V. Savinov

PROBLEMS involving the dynamic accuracy of automatic control systems are gaining importance steadily because of the more exacting engineering requirements imposed on such systems. In this context, particular interest centers on a buildup of perturbations, a problem that was posed and solved for linear systems by Bulgakov and developed further in subsequent work by Roitenberg, Kuzovkov, and others.[1–4]

The present paper deals with a dynamical system subjected over a finite time interval to the action of perturbing forces bounded in absolute value. We consider the determination of maximum deviation of any given coordinate of the dynamical system involved, the peak value being accumulated to some preassigned instant of time under the most unfavorable perturbation conditions.

The solution of this problem requires integration of an auxiliary system of differential equations, known as an adjoint system of equations—a task suited to analog computers.

The procedure followed in using analog computers to solve the problem of cumulative perturbations in linear and nonlinear systems, as well as the "hit" problem, which is strikingly similar in character to the problem of accumulated perturbations, will be outlined.

Translated from Vestnik Moskovskogo Universiteta, Seriia I: Matematika i Mekhanika (Bulletin of Moscow University, Series I: Mathematics and Mechanics), no. 3, 62–76 (1961). Translated by Faraday Translations, New York.

Solution by Analog Computer of the Problem of a Buildup of Perturbations in Linear Systems

Consider a dynamical system whose motion is described by the following linear differential equations with variable